

Charybdotoxin Unbinding from the *mKv1.3* Potassium Channel: A Combined Computational and Experimental Study

Morteza Khabiri,^{†,‡} Azadeh Nikouee,^{§,‡} Lukasz Cwiklik,^{||,⊥} Stephan Grissmer,[§] and Rüdiger Ettrich*,[†]

[†]Institute of Nanobiology and Structural Biology of GCRC, Academy of Sciences of the Czech Republic, and Faculty of Sciences, University of South Bohemia in Ceske Budejovice, Zamek 136, CZ-373 33 Nove Hrady, Czech Republic

[§]Institute of Applied Physiology, Ulm University, Albert-Einstein-Allee 11, 89081 Ulm, Germany

^{||}J. Heyrovsky Institute of Physical Chemistry, Academy of Sciences of the Czech Republic v.v.i., Dolejskova 3, 18223 Prague 8, Czech Republic

[⊥]Institute of Organic Chemistry and Biochemistry, Academy of Sciences of the Czech Republic and Center for Complex Molecular Systems and Biomolecules, Flemingovo nám. 2, 16610 Prague 6, Czech Republic

ABSTRACT: Charybdotoxin, belonging to the group of so-called scorpion toxins, is a short peptide able to block many voltage-gated potassium channels, such as *mKv1.3*, with high affinity. We use a reliable homology model based on the high-resolution crystal structure of the 94% sequence identical homologue Kv1.2 for charybdotoxin docking followed by molecular dynamics simulations to investigate the mechanism and energetics of unbinding, tracing the behavior of the channel protein and charybdotoxin during umbrella-sampling simulations as charybdotoxin is moved away from the binding site. The potential of mean force is constructed from the umbrella sampling simulations and combined with K_d and free energy values gained experimentally using the patch-clamp technique to study the free energy of binding at different ion concentrations and the mechanism of the charybdotoxin–*mKv1.3* binding process. A possible charybdotoxin binding mechanism is deduced that includes an initial hydrophobic contact followed by stepwise electrostatic interactions and finally optimization of hydrogen bonds and salt bridges.



INTRODUCTION

Potassium channels are representing the most diverse group of membrane integral proteins. The presence of potassium channels is not confined to excitable cells such as muscle cells and neurons. However, they have a variety of roles in nonexcitable cells, such as pancreatic β -cells, lymphocytes, and fat cells.^{1–4} The *mKv1.3* potassium channel, which is expressed in T-lymphocyte cell membranes, is a member of *Shaker*-related voltage-gated potassium channels. This type of delayed rectifier channel is assembled from four identical subunits.⁵ All four monomers contain six membrane spanning α -helices. The central pore of the channel is formed from S5 and S6 linkers, transmembrane segments, and the p-loop of each monomer. The ion conduction pathway contains the conserved TVGYG sequence, which has a critical role in potassium selectivity.⁶ It has previously been reported that blocking the Kv1.3 potassium channel can reduce cytokine production and T-cell proliferation. This finding revealed that channel blockers are excellent candidates for managing autoimmune diseases.^{7–10} Scorpion toxins, which block K^+ channels with 1:1 stoichiometry, are one of the most potent potassium channel blockers.¹¹ They can be considered a template for drug design in the treatment of autoimmune diseases. Therefore, understanding the exact details of the interaction between K^+ channels and scorpion toxins is highly valuable to researchers.^{12–16} Charybdotoxin (ChTX), a member of the scorpion toxins family, is a well-known blocker of

potassium channels. The ChTX primary structure contains 37 amino acids, seven of which are charged. This includes four lysine residues (K11, K27, K31, and K32), three arginine residues (R19, R25, and R34), and one negatively charged glutamic acid residue (E12). Since the N terminus of the toxin starts with an uncharged residue (pyroglutamic acid), ChTX has a net charge of +5e, which is critical for effective electrostatic interactions between the channel and the toxin. The secondary structure of this peptide toxin consists of one α -helix and three β -strands, and 3D structure is stabilized by three disulfide bridges.^{17–23} Several pieces of evidence indicate that K27 acts as a key residue for blocking the central pore of the channel.²⁴ A couple of studies focusing on the effect of mutations on the interactions between ChTX and different K^+ channels have provided preliminary information about which interactions are critical and potent.^{24–28} Nevertheless, this information still does not give a full understanding of the toxin binding and unbinding mechanism. Further experiments indicated that many factors are involved in the affinity of scorpion toxins to potassium channels, such as the distribution of charges on the surface of the toxin or the channel, the dipole moments of the toxin and the channel, and the ionic strength.

Received: June 30, 2011

Revised: August 30, 2011

Published: August 30, 2011

Giangiacomo et al.,²⁹ Fremon et al.,³⁰ Blanc et al.,^{31,32} and MacKinnon and Miller¹¹ reported that ChTX has a lower affinity in the presence of potassium ions due to the trans knock-off of ChTX by K⁺, probably because K⁺ might destabilize bound toxin and increase the dissociation rate of ChTX.²⁷ Also the existence of a nonspecific encounter complex in the initial diffusional step has been proposed that would precede the actual specific binding event.³³ Although to date the three-dimensional structures of a toxin–channel complex has been determined experimentally only in two cases, a chimeric KcsA–Kv1.3 with bound KTX³⁴ and KcsA with bound ChTX,³⁵ a variety of computational methods were applied to investigate the mechanistic details of the interaction between several scorpion toxins and different potassium channels. Hereby, toxin association and dissociation processes were studied using homology modeling and docking,^{25,36,37} Brownian dynamics (BD),³⁷ long-time molecular dynamics (MD) simulations and free energy surfaces,³⁸ generalized Born (GB) solvent model to score structures versus the Poisson method (MM/GB-SA),³⁹ umbrella sampling and potential-of-mean-force (PMF).^{36,40} Interactions between the toxin and the channel were described in several studies,^{25,37,41} and it has been proposed that the electrostatic interactions are the dominant governing component for toxin–channel binding.⁴² Residues Lys27, or Arg25 from ChTX, and Tyr400, Asp402, His404, Asp386, and Gly380 in each subunit of the *m*Kv1.3 potassium channel were identified as the key residues for toxin–channel recognitions.^{25,37} So far, to the best of our knowledge, there is only one study about binding free energy calculation of a toxin–channel that is ChTX in complex with the KcsA potassium channel,³⁶ and no data were reported regarding ChTX and voltage-gated channels. Hence, in the present study we have investigated the details of the interactions between ChTX and the voltage-gated *m*Kv1.3 channel, particularly focusing on the unbinding process in a solution containing high and low K⁺ concentration.

The 94% sequence identity with the structural homologue Kv1.2 enables us to generate a reliable homology model based on its high-resolution crystal structure (PDB code, 2A79). Charybdotoxin (PDB code, 2CRD) docking was followed by embedding the whole channel into a palmitoyloleoyl phosphatidylcholine (POPC) membrane bilayer and solvating the embedded structure in SPC/E water with high- and low-molar KCl. Molecular dynamics simulations were run to investigate the mechanism and energetics of unbinding, tracing the behavior of the channel protein and charybdotoxin during umbrella sampling simulations as charybdotoxin is moved away from the binding site. The potential of mean force for the unbinding of charybdotoxin is constructed from the umbrella sampling simulations by the weighted histogram method and used to calculate the binding free energy of the toxin. To confront the theoretical results of the PMF calculations with experimental values, the dissociation constant (K_d) was measured using the patch-clamp technique and translated into an experimental value for the free energy of binding. By comparing residues that we identified as interacting during the unbinding process with key residues reported in previous studies, we were able to deduce the possible charybdotoxin binding mechanism.

MATERIAL AND METHODS

Experiment. *Cells.* All experiments were carried out on a cell line stably expressing *m*Kv1.3 channels.⁴³ The cells were maintained in a culture medium of Dulbecco modified eagle medium

(MEM) supplemented with 10% fetal bovine serum and G418 antibiotics in a humidified, 5% CO₂ incubator at 37 °C.

Chemicals and Solutions. All experiments were performed in solution containing an external mammalian Ringer's bath of either high [K⁺]_o (KRi, potassium ringer), containing 164.5 mM KCl, 2 mM CaCl₂, 1 mM MgCl₂, and 5 mM HEPES, or low [K⁺]_o (NaRi, sodium ringer), containing 160 mM NaCl, 4.5 mM KCl, 2 mM CaCl₂, 1 mM MgCl₂, and 5 mM HEPES. The osmolarities of the solutions were between 290 and 320 mOsM, and the pH was adjusted to pH 7.4 with HCl. The internal pipet solution, [KF]_i, contained 155 mM KF, 2 mM MgCl₂, 10 mM EGTA, and 10 mM HEPES. The osmolarity of the [KF]_i solution was between 290 and 320 mOsM, and the pH was adjusted to pH 7.2 with KOH. Lyophilized samples of ChTX (Latoxan, Valence, France; Bachem, Bubendorf, Switzerland) were kept at -20 °C, and final dilutions were prepared before measurements in the external bath solutions containing 0.1% bovine serum albumin (Sigma-Aldrich Chemie, Steinheim, Germany).

Electrophysiology. All experiments were carried out using the whole-cell recording mode of the patch-clamp technique⁴⁴ at room temperature (18–22 °C). We used a simple syringe-driven perfusion system to exchange the bath solution in the recording chamber. Electrodes were pulled from glass capillaries (Science Products, Hofheim, Germany) in three stages and fire-polished to resistances measured in a bath of 2–4 MΩ. Membrane currents were measured by an EPC-9 patch-clamp amplifier (HEKA Electronik, Lambrecht, Germany) interfaced to a PC running acquisition and analysis software (Patchmaster/Fitmaster v2.00). All currents were filtered by a 2.9 kHz Bessel filter and recorded with a sampling frequency of (1–5 kHz). Series resistance compensation (75–80%) was used if the current exceeded 2 nA. Capacitive and leak currents were subtracted according to the P/10 procedure. Data were analyzed by Igor Pro 3.12 (Wave Metrics, Lake Oswego, OR, USA) and Microsoft Office Excel 2007.

Model System and MD Simulations. *Homology Modeling.* Since the crystal structure of the human voltage-gated potassium channel Kv1.3 has not yet been determined, the three-dimensional model of the *m*Kv1.3 was constructed using the crystal structure of Kv1.2 (PDB code, 2A79) with 2.9 Å resolution as a template. Voltage-gated potassium channels are comprised of six transmembrane segments and one pore loop. The first four *m*Kv1.3 transmembrane helices (S1–S4) enable the channel to sense and respond to changes in membrane potential⁴⁵ and are only involved in the detection of changes in the membrane potential, rendering the channel in an open or closed state.⁴⁶ The homologous KcsA potassium channel structure contains only M1/M2 helices (which equals S5 and S6 in Kv1.3 channels) and the pore loop between,⁶ indicating that for conduction S5/S6 helices are essential, and earlier molecular dynamics studies on Kv1.3 demonstrated the structural stability of the tetrameric core made of S5-pore-S6.³⁷ However, for homology modeling we do not simply consider the S5/S6 helices of the *m*Kv1.3 channel, but to improve the stability even more we additionally added the S4 helix in our study. Finally, a structural model of *m*Kv1.3 S4/S5-pore-S6 was generated on the basis of the close homologue's Kv1.2 crystal structure using comparative modeling. This structure, when embedded into the POPC membrane, equilibrates after 2 ns, giving a root mean square deviation (rmsd) value of less than 1 Å from the initial model, staying stable over the time accessible by MD. Because no other transmembrane segments or extracellular parts are reported to participate in toxin–channel interactions, neither are found to do so in the experimentally

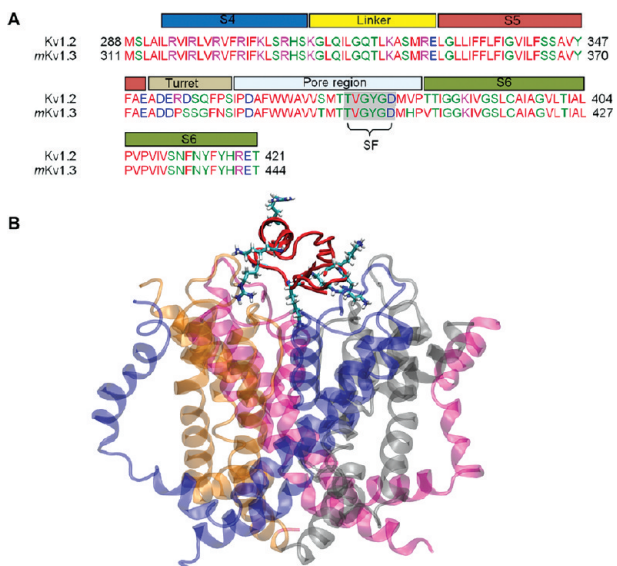


Figure 1. Amino acid sequence alignment of Kv1.2 and *m*Kv1.3 showing 94% sequence similarity. Docked ChTX with *m*Kv1.3 channel after 4 ns equilibration.

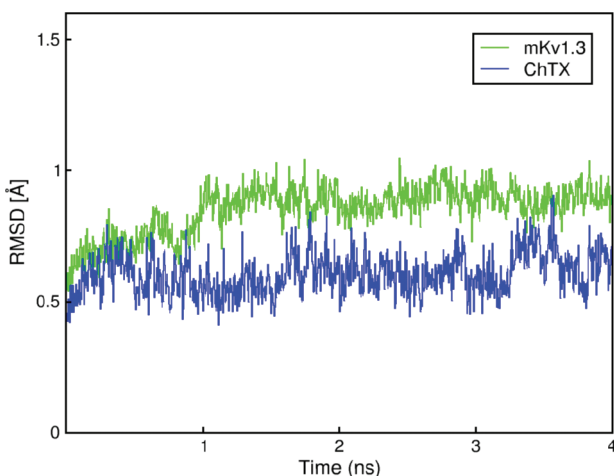


Figure 2. Root mean square deviation of the *m*Kv1.3 channel in complex with ChTX during the 4 ns equilibration period. Rmsd values less than 1 Å demonstrate the principal stability of the ChTX–*m*Kv1.3 complex.

determined 3D structures, we decided to use this stable segment for our calculations to keep the computational demand for the umbrella sampling as low as possible. Previously reported homology models of Kv1.3 structures were based on the crystal structure of KcsA.³⁷ However, the 30.93% sequence identity and 62.89% similarity between KcsA and Kv1.3 results in structural models with a very limited resolution, especially with respect to the side chains. As is depicted in Figure 1, the sequence alignment between *m*Kv1.3 and Kv1.2 in this region shows 94% sequence identity without any gaps, eliminating modeling errors coming from wrong sequence alignments or incorrect loop modeling in sequence variable regions or insertions. This close agreement allowed for the above-mentioned reasons the construction of a very reliable homology model of the voltage-gated *m*Kv1.3 potassium channel, comparable to the quality of the available crystal structure, and suitable for structural

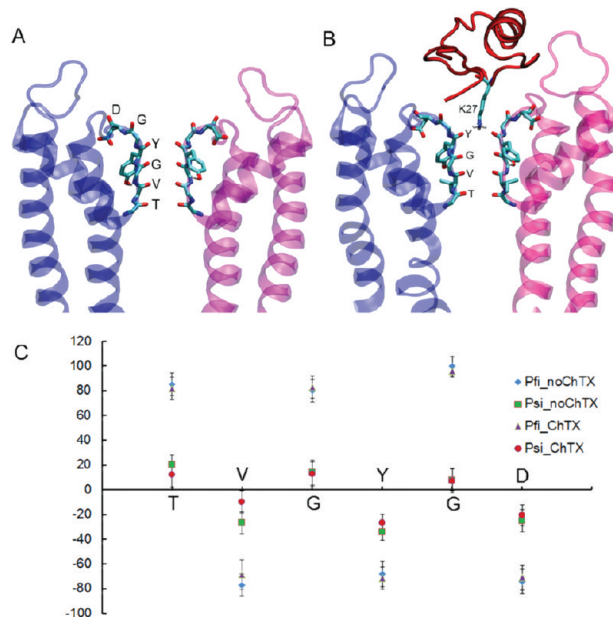


Figure 3. *m*Kv1.3 selectivity filter conformation before docking of ChTX (A) and in the ChTX–*m*Kv1.3 complex with K27 occluding the pore (B). Comparison of dihedral angles ϕ and ψ of selectivity filter residues before and after ChTX docking (C). Values for the docked conformation are from the last nanosecond of each simulation.

analysis, molecular dynamics simulations, and docking studies. Several three-dimensional models of the tetrameric S4/S5/S6 module of *m*Kv1.3 were built and examined by employing the Modeler 9v2 package.⁴⁶ The tertiary structure models were checked with Procheck,⁴⁷ and the most favored one was selected as the final model for embedding into the membrane.

Embedding Model Inside Membrane. The channel itself and the channel–toxin complexes resulting from the docking were embedded into a preequilibrated POPC bilayer, made from 512 phospholipid molecules, based on the 128 lipid bilayer provided by Tielemans et al.⁴⁸ using the INFLATEGRO method,⁴⁹ which relies on placing lipids and the protein on a widely spaced grid followed by “shrinking” the grid until the bilayer with the protein achieve the desired density. Simulations were performed with the GROMACS 4.0.7 software suite^{50,51} employing the all-atom force field of the OPLSAA type,⁵² adapted for POPC lipids on the basis of parameters of Berger et al.⁵³ and Marrink et al.⁵⁴ During this procedure the structure of the bilayer stayed mostly intact, reducing equilibration time. The resulting 498 lipid molecules were neatly packed around the protein. Because the *m*Kv1.3 model was constructed on the basis of the conductive form of the Kv1.2 channel,⁵⁵ before the final structures were solvated, three potassium ions were placed exactly in positions found in the crystal structure at sites S0, S2, and S4 inside the selectivity filter. Water molecules were placed at sites 1 and 3 as described in refs 56–58. It was assumed that the water density in the central cavity was the same as the density in the bulk solution.⁵⁹ After 1000 step minimization, the structure of the *m*Kv1.3 model system remained restrained and ran for 1 ns in order to equilibration between channel, water, and POPC membrane. Following 1 ns, the restraint was removed from the system and the system ran for 5 ns. The rmsd value less than 1 Å shows that channel structure is stable (data not shown). Finally, only the structure of *m*Kv1.3 resulting from the 5 ns molecular dynamics simulations with the selectivity

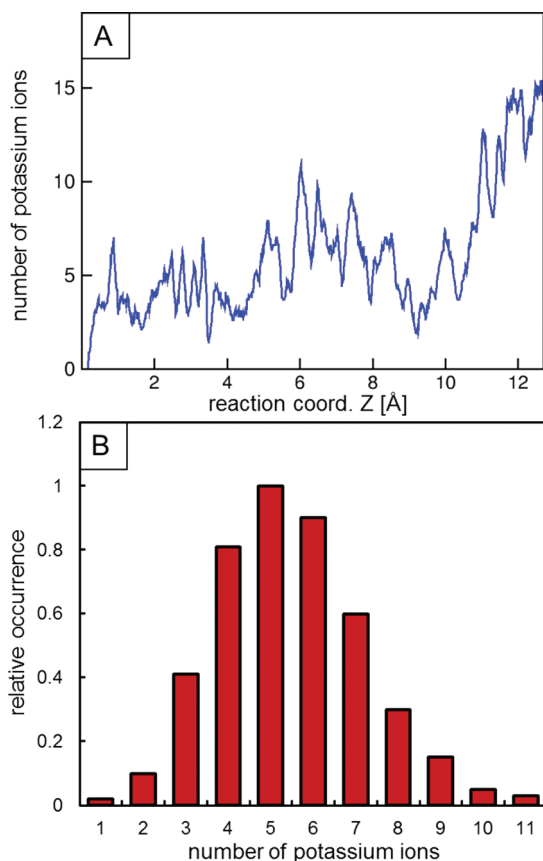


Figure 4. Number of potassium ions in a proximity of less than 10 Å from the channel during the unbinding process (A). The relative occurrence of potassium ions after unbinding of ChTX in a distance of less than 3.5 Å from the selectivity filter defined by Y400, G401, D402, M403, H404, and P405 pore region amino acids. In the histogram the relative numbers of K^+ within the 3.5 Å distance are shown. The relative occurrence values are normalized in order to get a unit value for the most probable number of K^+ . The histogram shows, on average, five ions in surface contact with the selectivity filter (B).

filter in a conductive form was chosen as the initial structure for docking.

Docking of ChTX to Kv1.3. The NMR structure of ChTX¹⁸ was extracted from the Protein Data Bank (PDB) database (PDB ID, 2CRD). Initially, ChTX was positioned manually close to the equilibrated model structures so that K27 was facing the pore and R25 was oriented toward channel residues D386 of one of the subunits, to match the data of Aiyar et al.²⁵ for Kv1.3 and interactions patterns coming from the determined structure of a potassium channel charybdotoxin complex.³⁵ Subsequently, ChTX was docked using local docking in AutoDock 4.0,⁶⁰ as implemented in YASARA Structure.^{61,62} The final docking results were then compared in detail to the docking results of ChTX–Kv1.3 previously reported by Yu et al.³⁷ and Aiyar et al.²⁵ and were found to be in good agreement (Figure 1).

Molecular Dynamics Simulations. The ChTX–mKv1.3 complex was solvated employing water molecules described by the extended simple point charge model of water.⁶³ Two systems were constructed, one with a low KCl concentration and the other with a high KCl concentration. In case of low salt concentration, only 21 chloride counterions were added to neutralize the system. In the case of high salt concentration, both potassium ions and chloride

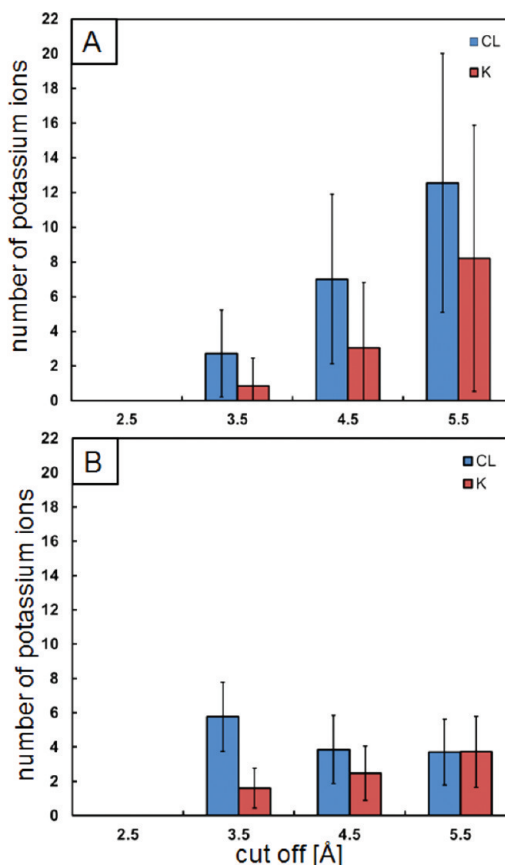


Figure 5. ChTX solvation shell in the vicinity of mKv1.3 channel (dissociated form) (A) and solvated alone (B) in 160 mM KCl solution. The number of ions in each cutoff was subtracted by the ions number from the previous cutoff.

ions were added to achieve a final salt concentration of 160 mM KCl and to achieve electric neutrality. As mentioned before, it was assumed that the water density in the central cavity was the same as the density in the bulk solution.⁵⁹ Molecular dynamics simulations were carried out in the isothermal–isobaric (NPT) ensemble employing a 2 fs time step. Periodic boundary conditions were used. Initial velocities were assigned by applying a Maxwell distribution at 300 K. The SETTLE and SHAKE⁶⁴ (nonwater) algorithms were used to constrain covalent bond lengths in water and non-water parts of the system, respectively. Lennard-Jones and electrostatic interactions were cut off at a distance of 10.0 Å, and the long-range electrostatic interactions were computed by employing the particle-mesh Ewald method.⁶⁵ The temperature was kept at 300 K by separately coupling the protein and solvent to an external temperature bath ($T = 0.1$ ps). The temperature coupling was achieved using The Nose–Hoover⁶⁶ algorithm. The pressure was kept constant at 1 bar by weak coupling ($T = 2.0$ ps) to a pressure bath using the Parrinello–Rahman algorithm,⁶⁷ which was employed with a semiisotropic mode. Since the presence of potassium ions inside the selectivity filter (SF) affects the conformation of the bound ChTX,³⁶ all potassium ions were removed from the SF. However, experimental results demonstrated that a single potassium cation occupies the S4 position in the SF³⁵ in the presence of ChTX. To mimic this effect of potassium on the structure of the SF, a harmonic constraint with the force constant of 2.5 (kcal/mol)/Å², which

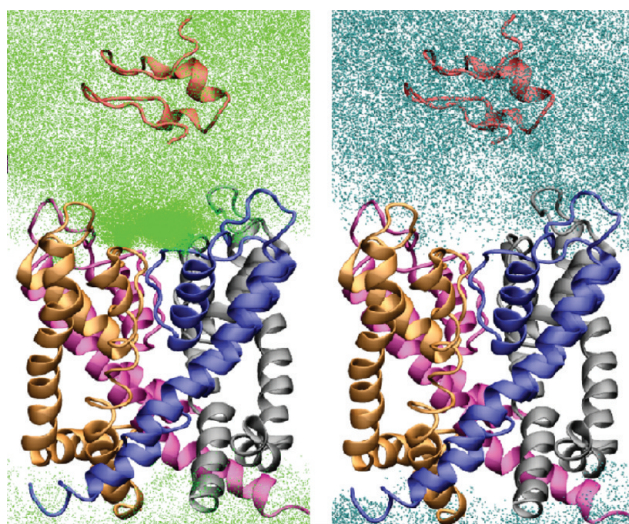


Figure 6. Positions of K^+ and Cl^- in the unbinding process for high K^+ concentration. All positions that either K^+ (left, green) and Cl^- (right, cyan) were in during the whole simulation from all umbrellas are shown. Both ChTX and channel geometries are taken from the last snapshot of the last umbrella sampling window. For clarity, S4 helices are not shown.

corresponds to the force induced by K^+ inside the SF,⁶⁸ was employed to restrain $\text{C}\alpha$ of TVG amino acids, corresponding to the S4 position, in the selectivity filter.

Umbrella Sampling and Potential of Mean Force Calculations. The free energy profile of ChTX unbinding was estimated by employing the PMF method with umbrella sampling. Umbrella sampling simulations were performed with the harmonic biasing potential acting along the membrane normal. The method was set up as described by Chen and Kuyucak.³⁶ The distance between the center of mass of ChTX and the membrane was sampled with roughly 0.5 Å intervals via steered MD simulations over a 13 Å path in the z direction. For the window generation ChTX is pulled with 5 (kcal/mol)/Å² at the speed of 5 Å/ns for 3 ns. A total of 26 windows, with an extra 10 windows to improve the sampling in selected regions, was collected. The windows were numbered from 0 to 26, with 0 representing the window for the ChTX–mKv1.3 complex. For each of these windows, the system was subjected to a 4 ns umbrella sampling MD simulation with the force constant of 50 (kcal/mol)/Å² applied to the center of mass of ChTX. Afterward, the weighted histogram analysis method (WHAM),⁶⁹ which is included in the GROMACS suite, was employed to calculate the free energy profile of the unbinding of ChTX from the membrane protein.

RESULTS AND DISCUSSION

Since voltage-gated potassium channels Kv1.2 and mKv1.3 are remarkably similar in their sequence, with 94% identical residues in the primary sequence, we constructed a three-dimensional model of mKv1.3 that is comprised of three transmembrane helices, S4, S5, and S6, and the pore region (p-loop) according to Kv1.2 crystal structure (Figure 1). In this model the SF adapted its conductive conformation (Figure 3) and ChTX was docked on the basis of well-characterized ChTX–Kv1.3 interactions, which were previously identified by mutant cycle analyses and electrostatic compliance experiments²⁵ as well as previous computational studies.^{37,70,71} Additional information about the general interaction patterns of charybdotoxin with ion channels is

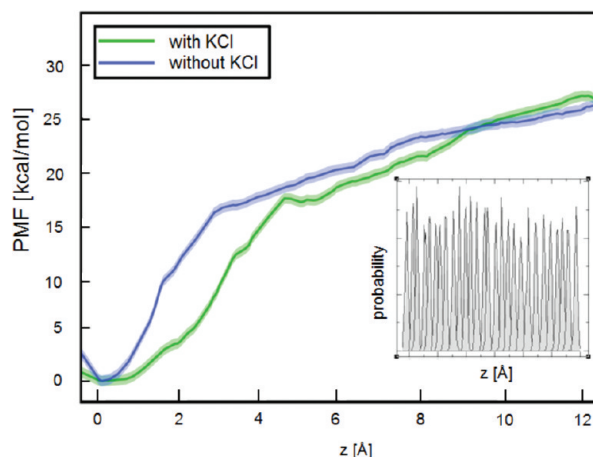


Figure 7. Comparison of the PMFs obtained from the umbrella sampling simulations of ChTX–mKv1.3 in high- and low-molar KCl using the force constants of 50 (kcal/mol)/Å². Overlapping between the individual umbrella sampling histograms is depicted in the inset for the high-molar KCl system and is qualitatively similar for low-molar KCl. By considering the error bars, free energy values in both cases are the same.

coming from the determined structure of a potassium channel–charybdotoxin complex.³⁵ The final docked conformation shows ChTX sitting right above the selectivity filter, similar to what is seen in the crystal structure of the KcsA–ChTX complex.³⁵ The rmsd of less than 1 Å for $\text{C}\alpha$ from the initial coordinates during the 4 ns equilibration simulation that followed the docking shows that there is no significant conformational change or induced fit in the structure of mKv1.3 or ChTX (Figure 2), demonstrating the principal compatibility of the selected conformations and the stability of the docking. To determine the conformation of the selectivity filter³⁴ after the equilibration and to explore the possibility that its structure might be affected by ChTX binding, we measured the ϕ and ψ angles for the selectivity filter region (TVGYGD) without and with ChTX binding (in both cases, from the last 1 ns of 4 ns equilibration). The differences between both angles before and after binding of ChTX are all within error (Figure 3C), which means that the selectivity filter is kept in its conducting conformation also in complex with the ChTX (Figure 3A,B). The last snapshot from the equilibration simulation was used as the initial conformation for the next simulation, which was run in order to investigate the unbinding process and to be able to perform free energy calculations. We ran two sets of directed MD simulations using low-molar and high-molar KCl in the solvent to explore the effect of low and high concentrations of potassium and chloride ions on toxin–channel interactions. Umbrella windows were at 0.5 Å intervals, and the same harmonic forces were used for both sets. In the simulations potassium ions, due to the negatively charged surface of the Kv1.3 channel, gradually start to take the place of ChTX during the unbinding process, eventually covering the channel surface. Figure 4A shows the number of potassium ions located within a distance of 10 Å from the atom nuclei on the channel's surface during the course of the unbinding process. Because we do not calculate a real molecular surface nor subtract the van der Waals radii, a potassium ion with surface contact could not get closer than approximately 3.5 Å, if measuring the atom distance by this method, and we can consider a 3.5 Å distance for ions being in surface contact. With ChTX unbinding and getting farther from the channel's surface, the number of potassium ions on the surface is increasing. Since

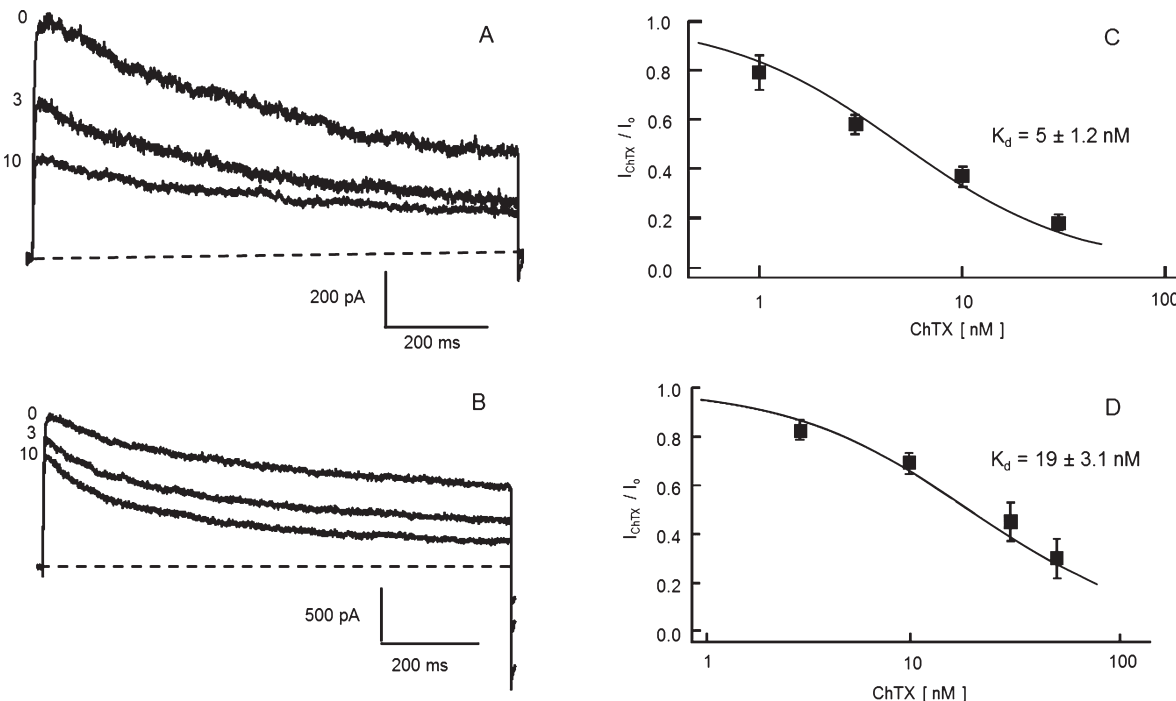


Figure 8. Left: Effect of ChTX on current through *mKv1.3* channels in Kri (potassium ringer) (A) and NaRi (sodium ringer) solution (B). Currents were elicited in the whole-cell configuration by 1 s depolarizing pulses to +40 mV from a holding potential of 80 mV every 30 s before and after application of 3 and 10 nM ChTX. Right: Dose–response curves of ChTX to block current through *mKv1.3* channels in Kri (potassium ringer) (C) and NaRi (sodium ringer) solution (D). K_d values were deduced by fitting a modified Hill equation ($I_{\text{ChTX}}/I_o = 1 - [1/[1 + ([\text{ChTX}]/K_d)]]$) to the data points obtained at different concentrations of toxins. I_o represents the peak current before and I_{ChTX} the peak current after ChTX application; [ChTX] is the concentration of ChTX in the external bath solution. All data points were obtained from at least five identical experiments and are given as mean \pm SD.

the channel surface close to the pore region consists mainly of negatively charged amino acids, potassium ions are strongly attracted to this part of the surface of the channel once the ChTX uncovers this area. To get more detailed information about the number of K^+ in contact with the pore region, we take into account only ions in a 3.5 Å distance from the closest atoms of amino acids Y400, G401, D402, M403, H404, and P405. The histogram (Figure 4B) reveals that there were on average five potassium ions in surface contact with the pore region. Once ChTX is fully dissociated from the channel, we would expect a ChTX hydration shell similar to the ChTX hydration shell in KCl solution. However, even though the ChTX lost practically all interactions with the channel by the end of the simulations, long-range electrostatics still might influence the hydration shell in its close proximity. Therefore we measured the number of ions in different distances from the ChTX. Again, the actual measured distances are between atom nuclei, so that a distance of around 3.5 Å corresponds to a surface contact. We find only three Cl^- and one K^+ in direct contact with the ChTX surface (Figure 5A), while ChTX simulated for 5 ns alone in 160 mM KCl solvent shows six Cl^- and two K^+ , and thus the expected difference between Cl^- and K^+ coming from the ChTX net charge (Figure 5B). In a distance from 3.5 to 4.5 Å we find seven Cl^- and three K^+ (Figure 5A), which is similar to the surface values for the solvated ChTX. However, when taking the distance from 4.5 to 5.5 Å, we already count K^+ that accumulated on the negative surface of the channel and the Cl^- in the next layer that were attracted by this positive charge. For ChTX alone in 160 mM KCl solution the number of ions is decreasing with increasing distance, and already

Table 1. Dissociation Constant and Free Energies of Binding for ChTX Binding to *mKv1.3* in Different Solvents

| medium | $K_d(\text{expt})$ (nM) | $\Delta G_b(\text{expt})$ (kcal/mol) | $\Delta G_b(\text{pmf})$ (kcal/mol) |
|----------------|----------------------------|---|--|
| low-molar KCl | 5 ± 1.2 | -11.4 ± 0.2 | -26 ± 1 |
| high-molar KCl | 19 ± 3.1 | -10.6 ± 0.2 | -27 ± 1 |

at a distance from 4.5 to 5.5 Å we find a homogeneous distribution of K^+ and Cl^- , as expected in a 160 mM KCl solution. In Figure 6 all positions that either K^+ (left) or Cl^- (right) took in the course of the complete unbinding process in high-molar KCl solution are shown. During the unbinding process Cl^- never occurred in a proximity to the pore surface (Figure 6, right), while K^+ where preferably occupying this region (Figure 6, left).

So far, only general aspects of the unbinding process of ChTX from *mKv1.3* were considered. To identify the influence of potassium ions on the ChTX–*mKv1.3* complex, we performed free energy calculations on the system using the PMF method. We considered two situations in our simulations, a 160 mM KCl solution that resembles a high K^+ concentration and pure water with a few chloride counterions to neutralize the system (no K^+), resembling an extremely low K^+ concentration. Interestingly, the results showed no difference between the total unbinding free energy of ChTX in water and in KCl solution (Figure 7). Previously, experimental studies have shown that the presence of potassium ions in solution reduces the affinity of binding of KTX to Kv1.3 by ~6-fold,²⁶ but there is no experimental data that show

the effect of ions on the interaction of ChTX to *m*Kv1.3 channels. To support our unexpected results of the PMF calculations, experimental work was performed in order to characterize the effect of externally applied ChTX on the current of *m*Kv1.3 channels. The experiments were carried out in solutions containing either high or low K⁺ concentration. We used a whole-cell recording mode to measure the current in the absence and presence of various concentrations of ChTX in low, 4.5 mM [K⁺]_o (NaRi), and high, 164.5 mM [K⁺]_o (KRi), solution (Figure 8A,B). The dose-response curves in Figure 8C,D, show that the affinity of ChTX to *m*Kv1.3 decreases with increasing potassium ion concentration in the solution. The value of *K*_d was calculated by fitting a modified hill equation to the data points. The *K*_d value was found to be of the same order, with 5 ± 1.2 nM in a solution with low [K⁺]_o and 19 ± 3.1 nM in a solution with high [K⁺]_o (Figure 8C,D). The slight increase of the *K*_d of ChTX to *m*Kv1.3 channels at a higher K⁺ concentration results in a very minor decrease of the ability of ChTX to block the current through the *m*Kv1.3 channels with ChTX still having a high enough affinity to block the current through the channel. Table 1 contains the absolute binding free energy obtained from both, high and low salt, PMF calculations, and the experimentally determined *K*_d values. In both cases, calculation and experiment, there is merely no difference between the free energy of ChTX unbinding in low and high K⁺ concentration with values around ~1 kcal/mol. In this respect, the measured and calculated free energies fully agree. However, the absolute values obtained from PMF calculations are ~15 kcal/mol higher than those experimentally measured, which could be rationalized by the different salt concentrations employed. Namely, in the experiment a mixture of sodium and potassium salt was used with either high or low ratio of potassium to sodium, which is necessary for keeping the pressure in the cell constant and a standard setup for those kinds of experiments. Note that *m*Kv1.3 is selective for K⁺; therefore, we do not expect Na⁺ to affect significantly the Kv channel structure.⁷² In the calculations, we modeled the high and

low potassium content by using either 160 mM KCl or pure water with counterions only. Thus, the ionic strength was different between experiment and calculations. An increased value for the calculated free energy difference compared with the experimental result was already seen in ChTX and KscA PMF calculations by Chen and Kuyucak.³⁶ However, the comparison between experimental and computational data allows one to conclude that the value of the binding free energy is independent of the external potassium concentration. While the free energy curves calculated with the PMF method for both solutions are in good agreement at large distances, they exhibit a slightly different behavior at a distance of 1–5 Å when the toxin is still close to the channel surface (Figure 7). In this region, the toxin is losing the main electrostatic interactions with the channel. Single amino acid that potentially might contribute to interactions between ChTX and the channel in PMF can be identified by measuring the residue-pair distances for each interaction point. Figure 9 shows the minimum distances of the center of mass of each toxin residue to the channel in the first umbrella sampling window. Fifteen residues are located in a distance as close as 2 Å from the channel. Among them, residues Q18 and S24 do not have any particularly strong interaction with the channel. The reason for them being close to the channel is their vicinity to the interaction residues nearby. The other 13 residues are potentially interacting and are shown in Table 2; their behavior was monitored during the unbinding process. Except for H21 and N22, experimental data are available, ascribing them a significant role in the K⁺ channel blocking. Point mutations of T23D and F2A²¹ have shown a modest decrease in the ChTX binding affinity to block shaker³⁵ and Ca²⁺-activated K⁺ channels,²¹ respectively. In our simulations both residues F2 and T23 have hydrophobic interactions with the channel. A point mutation from lysine to arginine in position 11, K11R, strengthens the ChTX interaction by 2.5-fold.²⁸ K11 in our simulations forms a hydrogen bond with the backbone oxygen of S379.

Another point mutation, N30G, weakens the ChTX interaction by 1000-fold in the presence of shaker channels.²⁸ The amide group of N30 in our simulations contacts the backbone oxygen of S378. R25 is very sensitive to the external K⁺ concentrations, which was demonstrated by varying the external K⁺ concentrations from 2 to 100 mM for wild type as well as for point mutations to D or Q at this position.²⁷ In the simulations the guanidinium group of ChTX–R25 bridges to D386 and D402. K27 has a key role in blocking the K⁺ channel and is very sensitive to the K⁺ passage through the selectivity filter.²⁷ A K27N mutant reduced ChTX potency by 300-fold.²⁵ ChTX–K27 extends into the selectivity filter and contacts the oxygens of the carbonyl groups of Y400 of all four chains in the channel in the simulations. Y36 has a unclear role in ChTX interaction, as different mutations show different effects at this position. While Y36F mutation does not have an effect on channel blocking, Y36N decreased the affinity 20-fold, whereas Y36A, Y36H, and Y36P abolish blocking activity.²¹ In the simulations Y36 has a hydrogen bond with the carboxyl group of D386. Mutants M29L²¹ and R34Q²⁷ decreased the ChTX off-rate from the shaker channel.^{21,27} In addition, between the side chains of both key residues, R25 and K11, is kept the aromatic ring of ChTX–W14,

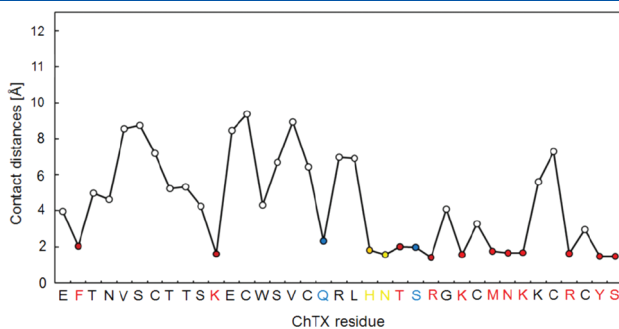


Figure 9. Average distances of ChTX residues to the channel in the ChTX–*m*Kv1.3 complex. The measured distances are the average minimum distances between the center of mass of each individual toxin residue and the channel in the first window of the umbrella sampling. Residues without a specific interaction but close to the channel surface are shown in blue, residues having specific interactions in our simulations that lack experimental verification are shown in yellow, and residues having specific interactions in our simulations and available experimental data are shown in red.

Table 2. Major Interactions between Pairs of Amino Acid Residues of ChTX and *m*Kv1.3 While ChTX Is Blocking the Channel

| ChTX | F2 | K11 | H21 | N22 | T23 | R25 | K27 | M29 | N30 | K31 | R34 | Y36 | S37 |
|-------|---------|---------|---------|---------|---------|----------------|----------------|----------|---------|----------|----------|---------|---------|
| Kv1.3 | S378(A) | S379(D) | G380(D) | P377(B) | G380(C) | D402, D386 (A) | Y400 (A,B,C,D) | H404 (D) | S378(D) | D402 (D) | S378 (A) | D386(C) | K411(A) |

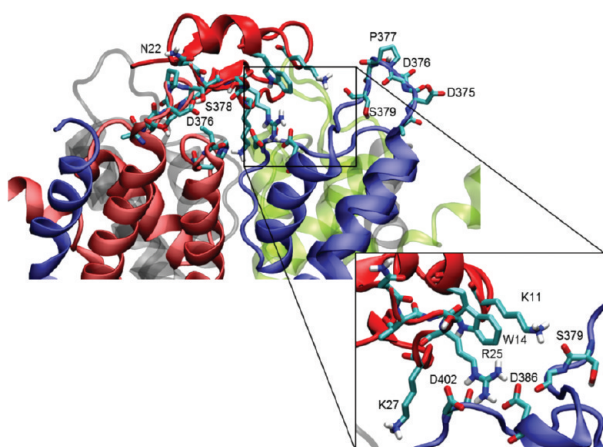


Figure 10. Key interactions between ChTX and *mKv1.3*. The magnified cubic box highlights the electrostatic interaction of R25 with D386 and D402 and of K11 with S379.

such as in a sandwich, constraining the ChTX to a particular structural conformation (Figure 10).

During the dissociation process these interactions between ChTX residues and the channel were monitored in both, high and low K^+ concentrations. Several of the interactions are affected by the presence of K^+ . Several hydrophobic and electrostatic interactions between ChTX and the channel seem to have an important role in the PMF. While R25–D386 and K31–D402 maintain their interactions until 3 Å on the reaction coordinate in low-molar KCl, they lose their interaction earlier in high-molar KCl (Figure 11B,D). Probably, this could be the major reason why the PMF has a steeper rise in low than in high K^+ concentration. On the other hand, the K27–Y400 interaction is maintained until 6 Å in high-molar KCl concentration, though with a higher flexibility; in low K^+ concentration it loses its firm contact around ~4 Å. When comparing the individual interacting residue-pair distances with the PMF graph, the steep rises of PMF in the 0–3 Å reaction coordinate in low-molar KCl is related to the destabilization of the interactions between F2–S378, N22–P377, R25–D386, K27–Y400, M29–H404, N30–S378, K31–D402, R34–S378, and S37–K411 (Figure 11). The remaining contacts get lost gradually roughly after 6 Å. In high-molar KCl, except for R25–D402, M29–H404, and R34–S378 which keep their interaction strongly until around 6 Å, the interactions are weakened after 1–2 Å. Moreover, some of the residues are able to establish a new interaction with other surface residues after losing their original interaction with the channel. For instance, once K27 looses its interaction with Y400, it gets in contact with G401 and mainly D402. These alternative interactions result in the smoother rise of the PMF after its initial steep rise in both high- and low-molar KCl. Besides this, the presence of ions in the solution influenced the unbinding process, as the potassium ions compete with the toxin for the negative charge of the carboxyl group of aspartic acid and the carbonyl group of the pore region amino acids. This effect is more obvious in 1–5 Å. The competition between K^+ ions and negatively charged groups on the channel surface is demonstrated by measuring the radial distribution function (RDF) of potassium ions around the center of mass of two groups of atoms (Figure 12): the guanidinium group of R25 in contact with D402 and D386 carboxylic groups as one group and the amino group of K11 in contact with S397

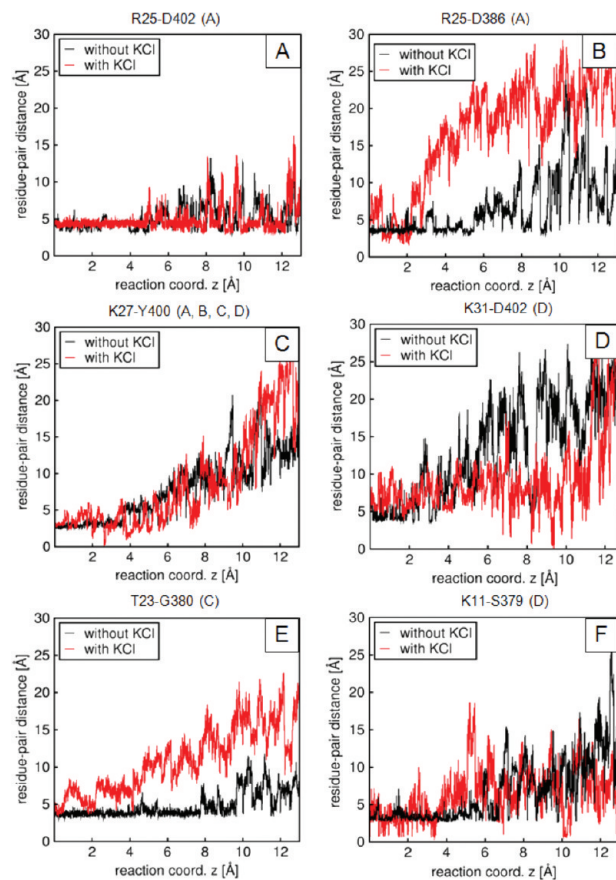


Figure 11. Contact distances between selected key residues of ChTX and *mKv1.3* during unbinding. Unbinding is expressed as the ChTX position along the reaction coordinate in the *z* direction. The CZ atom of the arginine guanidinium group, oxygens of the carboxylic group of aspartic acid, the NZ atom of the amide group in lysine, the threonine methyl group, and the oxygen of the serine hydroxy group were considered for measuring the distances.

carbonyl group as the second group. Figure 12 shows that the potassium ions are attracted by S379, D402, and D386 in the channel, replacing residues R25 and K11 of ChTX, when the ChTX–channel interactions are already weakened by the larger distance.

Umbrella sampling gives a good opportunity to understand in detail the behavior of ChTX itself during unbinding from the *mKv1.3* channel. A comparison with available experimental data confirms H404, D386, and G380, which are located in the pore region, to be involved in channel sensitivity to toxin.²⁵ D402, placed right at the upper part of the selectivity filter, modulates the inactivation process.⁷³ The strong interactions of toxin residues R25 and K31 with this amino acid will probably affect the flexibility of the selectivity filter, guiding this modulation. MD simulations of ChTX unbinding in the course of umbrella sampling show that ChTX does not lose all of its interactions with the channel at the same time during the unbinding process. ChTX still maintains the interactions of residues K11, R25, and N22 while other contacts are becoming detached. These three amino acids act as a hinge during the unbinding process, which makes ChTX unbinding resemble the opening of the lid of a pitcher. Figure 13 shows the conformation of the ChTX when losing all main interactions with the channel. Figure 13A shows the

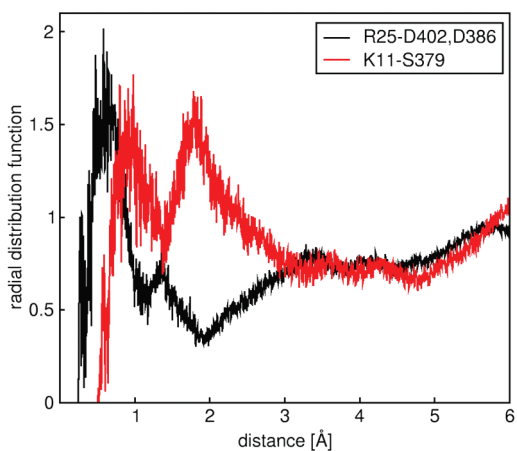


Figure 12. Radial distribution function of K^+ when the toxin is bound to the channel. The rdf is measured around D402 and D386, which are interacting with R25, and around the Ser379 carbonyl oxygen group when interacting with K11. Hereby, the rdf was measured while the ChTX–*mKv1.3* complex was solvated by water and ions in the high K^+ concentration in the bulk KCl solution, and data were taken from the second umbrella (reaction coordinate, 0.5 Å) to monitor the situation when the ChTX–channel interactions are already weakened by the slightly larger distance.

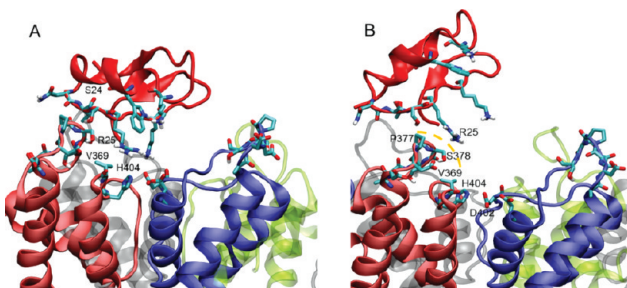


Figure 13. ChTX after the loss of short-range electrostatic interaction with the channel. Only hydrophobic interactions are left (A). The hydrophobic patch (yellow dashed line) which is created by V369, S378, and P377 (B).

conformation of ChTX when ChTX–R25 loses its interaction with both aspartic acid residues. In the next step the guanidinium group of ChTX–R25 flips into a horizontal conformation with respect to the channel surface and is thus placed in close proximity to H404, forming a hydrogen bond, and at the same time having a hydrophobic contact with the methyl group of V369. Finally, the only direct contacts left are weak hydrophobic interactions of ChTX with the channel, and thus, once all short-range electrostatic interactions disappeared, ChTX unbinding proceeds easily.

CONCLUSION

In this paper, binding free energy and the unbinding process of ChTX from the *mKv1.3* voltage-gated potassium channel was investigated in the absence and presence of external potassium ions. In contrast with previously reported models, the high sequence identity and similarity of *mKv1.3* with Kv1.2 allows for a high-resolution homology model to study the ChTX–Kv1.3 complex interaction. Free energy calculations performed using the PMF method found no difference in free energy of the complex in

a solution with low versus high salt concentrations. Experimentally gained K_d values show a slightly weaker affinity of ChTX to *mKv1.3* in high K^+ concentration solution; however, free energy calculations based on these experimentally determined K_d values found only about 1 kcal/mol in difference between the free energy of the ChTX–Kv1.3 complex in a solution of low- versus high-molar concentration of KCl. However, the shape of the free energy curve obtained from PMF calculations shows that there is a difference in the unbinding behavior when comparing low and high ion concentration at a distance of 1–5 Å from the surface of the selectivity filter. Considering that the potassium ions occupy the pore region when ChTX is unbinding, their presence perturbed the ChTX unbinding process by establishing a network of interactions inbetween the ChTX and channel surfaces. However, if error is taken into account for both theoretical and experimental calculations, then the binding free energies found from PMF calculations and experimental measurements in the presence and absence of potassium ions are the same. We can conclude that while the presence of potassium ions might have a critical role in the diffusional step of the binding process, however, it does not have an influence on specific binding and the binding free energy. We found that the PMF method is not only a powerful tool to estimate the binding energy but it is also a reliable method to investigate the details of the toxin binding and unbinding process. Our molecular dynamics simulations demonstrate the significant role of R25 and K27 in ChTX and *mKv1.3* binding, which is in agreement with Rauer et al.⁷⁰ During unbinding, K27 loses its interaction earlier than R25 does. Moreover, during the unbinding process, the guanidinium group of arginine loses its interaction with D386 and D402 and forms a new hydrogen bond with H404. Finally, only weak hydrophobic contacts with the methyl group of V369 and the C β H2 group of S378 are left before losing the contact with the channel completely. Aiyar et al.²⁶ and Rauer et al.⁷⁰ have shown that the coupling of the side chains of R25 and H404 aligns the orientation of the toxin with the pore axis. Combining our experimental data with the theoretical results from molecular dynamics simulations of the ChTX unbinding process led us to a new hypothesis about the general mechanism of how ChTX binds to the Kv1.3 channel. Since the guanidinium group of R25 can have hydrophobic interactions on both sides and form a hydrogen bond on its plane edge,⁷⁴ it is a good candidate for the initial screening of the surface of the channel by the toxin. Once it comes in contact with the ring of P377, it is inevitable that the two residues will form a hydrophobic interaction. P377 is part of a larger hydrophobic patch including also C β H2 of S378 and the methyl group of V369. Initially, R25 only interacts with P377 and/or S378, but because hydrophobic interactions are nonspecific and can be considered as very weak, it eventually gets along the hydrophobic patch to finally reach H404 with its guanidinium group to form a hydrogen bond. As it approaches H404, R25 can also interact with the carboxylic acid group of D402 at the same time, bringing R25 in contact with D386 as well. As mentioned above, the side chains of R25, W14, and K11 are sandwiched by hydrophobic interactions that constrain them in parallel next to each other. Moreover, we think that hydrophobic interactions between the side chains of R25, W14, and K11 hold the conformation of ChTX in a specific structural state that helps K27 extend into the central pore of the channel. As a result of this interaction, K31 then has the opportunity to interact with D402 in the opposite monomer. In this situation, ChTX completely blocks the opening of the channel. The above-described key residue K11 is not present in KTX, the toxin reported to have the binding affected in high-molar KCl;²⁶ instead KTX has a

proline in the same position while the other interacting residues are mostly conserved. Also the mentioned W11 that is sandwiched between the K11 and R25 side chains is not present in KTX, but we find a leucine instead. Figure 11F shows that hydrogen bonding of K11 is not significantly altered in the presence of potassium, and thus K11 is probably the key difference between KTX and ChTX and the reason for the different binding modes of both toxins. This proposed mechanism of how ChTX blocks the potassium channel, which is based on our observations and interpretations of the unbinding process, is in good agreement with the reported as well as with previously published experimental results, and therefore might well reflect reality.

■ AUTHOR INFORMATION

Corresponding Author

*Tel.: +420386361297. Fax: +420386361279. E-mail: ettrich@nh.cas.cz.

Author Contributions

[†]These authors contributed equally to this work.

■ ACKNOWLEDGMENT

M.K. and R.E. acknowledge support from the Czech Science Foundation, Grant 203/08/0114, the Academy of Sciences of the Czech Republic, Grant AV0Z60870520, and the Ministry of Education, Youth and Sports of the Czech Republic, Grants LC06010 and MSM6007665808. S.G. and A.N. were supported by grants from the DFG (Gr 848/14-1). Additionally, M.K. was supported by the University of South Bohemia, Grant GAJU 170/2010/P. Access to the METACentrum computing facilities provided under the research intent MSM6383917201 is highly appreciated.

■ REFERENCES

- (1) Krasznai, Z. *Arch. Immunol. Ther. Exp.* **2005**, *53* (2), 127–135.
- (2) Hille, B. *Ionic Channels of Excitable Membranes*, 2nd ed.; Sinauer Associates: Sunderland, MA, 1992.
- (3) Chandy, K. G.; Gutman, G. A. Voltage-gated potassium channels. In *Ligand- and Voltage-Gated Ion Channels*; North, R. A., Ed.; CRC Press: Boca Raton, FL, USA, 1995.
- (4) Grissmer, S.; Dethlefs, B.; Wasmuth, J. J.; Goldin, A. L.; Gutman, G. A.; Cahalan, M. D.; Chandy, K. G. *Proc. Natl. Acad. Sci. U. S. A.* **1995**, *87*, 9411–9415.
- (5) MacKinnon, R. *Nature* **1991**, *350*, 232–235.
- (6) Doyle, D. A.; Morais Cabral, J.; Pfuetzner, R. A.; Kuo, A.; Gulbis, J. M.; Cohen, S. L.; Chait, B. T.; MacKinnon, R. *Science* **1998**, *280*, 69–77.
- (7) Chandy, K. G.; DeCoursey, T. E.; Cahalan, M. D.; McLaughlin, C.; Gupta, S. *J. Exp. Med.* **1984**, *160*, 369–385.
- (8) DeCoursey, T. E.; Chandy, K. G.; Gupta, S.; Cahalan, M. D. *Nature* **1984**, *307*, 465–468.
- (9) Freudenthaler, G.; Axmann, M.; Schindler, H.; Pragl, B.; Knaus, H. G.; Schütz, G. J. *Histochem. Cell Biol.* **2002**, *117*, 197–202.
- (10) Lewis, R. S.; Cahalan, M. D. *Science* **1988**, *239*, 771–775.
- (11) MacKinnon, R.; Miller, C. *J. Gen. Physiol.* **1988**, *91*, 335–349.
- (12) Koppenhofer, E.; Schmidt, H. *Pflügers Archiv-Eur. J. Physiol.* **1968**, *303*, 150–161.
- (13) Cahalan, M. D. *J. Physiol. (Oxford, U. K.)* **1975**, *244*, 511–534.
- (14) Simard, J. M.; Meves, H.; Watt, D. D. *Pflügers Archiv-Eur. J. Physiol.* **1986**, *406*, 620–628.
- (15) Wang, G. K.; Strichartz, G. R. *Mol. Pharmacol.* **1983**, *23*, 519–533.
- (16) Gonoi, T.; Hill, B. *J. Gen. Physiol.* **1987**, *89*, 253–274.
- (17) Anderson, C. S.; MacKinnon, R.; Smith, C.; Miller, C. *J. Gen. Physiol.* **1988**, *91*, 317–333.
- (18) Bontems, F.; Gilquin, B.; Roumestand, C.; Ménez, A.; Toma, F. *Biochemistry* **1992**, *31*, 7756–7764.
- (19) Sugg, E. E.; Garcia, M. L.; Reuben, J. P.; Patchett, A. A.; Kaczorowski, G. J. *J. Biol. Chem.* **1990**, *265* (31), 18745–18748.
- (20) Park, C. S.; Miller, C. *Biochemistry* **1992**, *31*, 7749–7755.
- (21) Stampe, P.; Kolmakova-Partensky, L.; Miller, C. *Biophys. J.* **1992**, *62* (1), 8–9.
- (22) Restrepo-Angulo, I.; Vizcaya-Ruiz, A. D.; Camacho, J. *J. Appl. Toxicol.* **2010**, *30* (6), 497–512.
- (23) Batista, C. V.; Gomez-Lagunas, F.; Rodriguez de la Vega, R. C.; Hajdu, P.; Panyi, G.; Gaspar, R.; Possani, L. D. *Biochim. Biophys. Acta* **2002**, *1601*, 123–131.
- (24) Park, C. S.; Miller, C. *Neuron* **1992**, *9* (2), 307–313.
- (25) Aiyar, J.; Withka, J. M.; Rizzi, J. P.; Singleton, D. H.; Andrews, G. C.; Lin, W.; Boyd, J.; Hanson, D. C.; Simon, M.; Dethlefs, B. *Neuron* **1995**, *15* (5), 1169–1181.
- (26) Aiyar, J.; Rizzi, J. P.; Gutman, G. A.; Chandy, K. G. *J. Biol. Chem.* **1996**, *271* (49), 31013–31016.
- (27) Goldstein, S. A.; Miller, C. *Biophys. J.* **1993**, *65* (4), 1613–1619.
- (28) Stocker, M.; Miller, C. *Proc. Natl. Acad. Sci. U. S. A.* **1994**, *91* (20), 9509–9513.
- (29) Giangiacomo, K. M.; Sugg, E. E.; Garcia-Calvo, M.; Leonard, R. J.; McManus, O. B.; Kaczorowski, G. J.; Garcia, M. L. *Biochemistry* **1993**, *32*, 2363–2370.
- (30) Fremont, V.; Blanc, E.; Crest, M.; Martin-Eauclaire, M. F.; Gola, M.; Darbon, H.; Van Rietschoten, J. *Lett. Pept. Sci.* **1997**, *4*, 305–312.
- (31) Blanc, E.; Lecomte, C.; Rietschoten, J. V.; Sabatier, J. M.; Darbon, H. *Proteins* **1997**, *277*, 29359–29362.
- (32) Blanc, E.; Sabatier, J. M.; Kharrat, R.; Meunier, S.; El Ayeb, M.; Van Rietschoten, J.; Darbon, H. *Proteins* **1997**, *29*, 321–333.
- (33) Escobar, L.; Root, M. J.; MacKinnon, R. *Biochemistry* **1993**, *32*, 6982–6987.
- (34) Lange, A.; Giller, K.; Hornig, S.; Martin-Eauclaire, M. F.; Pongs, O.; Becker, S.; Baldus, M. *Nature* **2006**, *440* (7086), 959–62.
- (35) Yu, L.; Sun, C.; Song, D.; Shen, J.; Xu, N.; Gunasekera, A.; Hajduk, P. J.; Olejniczak, E. T. *Biochemistry* **2005**, *44*, 15834–15841.
- (36) Chen, P. C.; Kuyucak, S. *Biophys. J.* **2009**, *96*, 2577–2588.
- (37) Yu, K.; Fu, W.; Liu, H.; Luo, X.; Chen, K. X.; Ding, J.; Shen, J.; Jiang, H. *Biophys. J.* **2004**, *86* (6), 3542–3555.
- (38) Woo, H. J.; Roux, B. *Proc. Natl. Acad. Sci. U. S. A.* **2005**, *102* (19), 6825–6830.
- (39) Lee, M. S.; Olson, M. A. *Biophys. J.* **2006**, *90* (3), 864–877.
- (40) Zhang, D.; Gullingsrud, J.; McCammon, J. A. *J. Am. Chem. Soc.* **2006**, *128*, 3019–3026.
- (41) Zachariae, U.; Schneider, R.; Velisetty, P.; Lange, A.; Seeliger, D.; Wacker, S. J.; Karimi-Nejad, Y.; Vriend, G.; Becker, S.; Pongs, O.; Baldus, M.; de Groot, B. L. *Structure* **2008**, *16* (5), 747–754.
- (42) Yi, H.; Qiu, S.; Wu, Y.; Li, W.; Wang, B. *BMC Struct. Biol.* **2011**, *11* (3), 1–9.
- (43) Grissmer, S.; Nguyen, A. N.; Aiyar, J.; Hanson, D. C.; Mather, R. J.; Gutman, G. A.; Karmilowicz, M. J.; Auperin, D. D.; Chandy, K. G. *Mol. Pharmacol.* **1994**, *45*, 1227–1234.
- (44) Hamill, O. P.; Marty, A.; Neher, E.; Sakmann, B.; Sigworth, F. J. *Pflügers Archiv-Eur. J. Physiol.* **1981**, *391* (2), 85–100.
- (45) Grottesi, A.; Sands, Z. A.; Sansom, M. S. *Curr. Biol.* **2005**, *15*, R771–R774.
- (46) Fiser, A.; Sali, A. *Methods Enzymol.* **2003**, *374*, 461–491.
- (47) Laskowski, R. A.; MacArthur, M. W.; Moss, D. S.; Thornton, J. M. *J. Appl. Crystallogr.* **1993**, *26*, 283–291.
- (48) Tieleman, D.; MacCallum, J.; Ash, W.; Kandt, C.; Xu, Z.; Monticelli, L. *J. Phys.: Condens. Matter* **2006**, *18*, 1221–1234.
- (49) Kandt, C.; Ash, W. L.; Tieleman, D. P. *Methods* **2007**, *41* (4), 475–488.
- (50) Berendsen, H. J. C.; van der Spoel, D.; van Drunen, R. *Comput. Phys. Commun.* **1995**, *91*, 43–56.

- (51) Lindahl, E.; Hess, B.; van der Spoel, D. *J. Mol. Model.* **2001**, *7*, 306–317.
- (52) Jorgensen, W. L.; Maxwell, D. S.; Tirado-Rives, J. *J. Am. Chem. Soc.* **1996**, *118*, 11225–11236.
- (53) Berger, O.; Edholm, O.; Jahnig, F. *Biophys. J.* **1997**, *72*, 2002–2013.
- (54) Marrink, S. J.; Berger, O.; Tieleman, D. P.; Jahnig, F. *Biophys. J.* **1998**, *74*, 931–943.
- (55) Long, S. B.; Campbell, E. B.; Mackinnon, R. *Science* **2005**, *309* (5736), 897–903.
- (56) Jensen, M. Ø.; Borhani, D. W.; Lindorff-Larsen, K.; Maragakis, P.; Jogini, V.; Eastwood, M. P.; Dror, R. O.; Shaw, D. E. *Proc. Natl. Acad. Sci. U. S. A.* **2010**, *107* (13), 5833–5838.
- (57) Hellgren, M.; Sandberg, L.; Edholm, O. *Biophys. Chem.* **2006**, *120* (1), 1–9.
- (58) Bernèche, S.; Roux, B. *Biophys. J.* **2000**, *78* (6), 2900–2917.
- (59) Charlotte, E. C.; Sansom, M. S. P. *J. Phys. Chem. B* **2002**, *106*, 4543–4551.
- (60) Morris, G. M.; Goodsell, D. S.; Halliday, R. S.; Huey, R.; Hart, W. E.; Belew, R. K.; Olson, A. J. *J. Comput. Chem.* **1998**, *19*, 1639–1662.
- (61) Krieger, E.; Darden, T.; Nabuurs, S. B.; Finkelstein, A.; Vriend, G. *Proteins* **2004**, *57* (4), 678–683.
- (62) Krieger, E.; Koraimann, G.; Vriend, G. *Proteins* **2002**, *47* (3), 393–402.
- (63) Berendsen, H. J. C.; Postma, J. P. M.; van Gunsteren, W. F.; Hermans, J. In *Intermolecular Forces*; Pullman, B., Ed.; D. Reidel: Dordrecht, The Netherlands, 1981; pp 331–342.
- (64) Ryckaert, J. P.; Ciccotti, G.; Berendsen, H. J. C. *J. Comput. Phys.* **1997**, *13*, 327–341.
- (65) Essmann, U.; Perera, L.; Berkowitz, M. L. *J. Chem. Phys.* **1995**, *103*, 8577–8592.
- (66) Noé, S.; Klein, M. L. *Mol. Phys.* **1983**, *50*, 1055–1076.
- (67) Parrinello, M.; Rahman, A. *J. Appl. Phys.* **1981**, *52*, 7182–7190.
- (68) Fururia, S.; Domenea, C. *Proc. Natl. Acad. Sci. U. S. A.* **2009**, *106* (38), 16074–16077.
- (69) Chodera, J. D.; Swope, W. C.; Pitera, J. W.; Seok, C.; Dill, A. K. *J. Chem. Theory Comput.* **2007**, *3* (1), 26–41.
- (70) Rauer, H.; Lanigan, M. D.; Pennington, M. W.; Aiyar, J.; Ghanshani, S.; Cahalan, M. D.; Norton, R. S.; Chandy, K. G. *J. Biol. Chem.* **2000**, *275* (2), 1201–1208.
- (71) Lipkind, G. M.; Fozard, H. A. *J. Membr. Biol.* **1997**, *158* (3), 187–196.
- (72) Nimigean, C. M.; Allen, T. W. *J. Gen. Physiol.* **2011**, *137* (5), 405–413.
- (73) Cordero-Morales, J. F.; Jogini, V.; Chakrapani, S.; Perozo, E. *Biophys. J.* **2011**, *100* (10), 2387–2393.
- (74) Heyda, J.; Mason, P. E.; Jungwirth, P. *J. Phys. Chem.* **2010**, *114*, 8744–8749.